Predicting Post-Procedural Complications Using MIMIC-III

Saeed Ul Hassan[1] and Faisal Maqbool[2]

Abstract— **To predict outcomes and take decisions for patients admitted in ICU requires specific features of medical records: worth, capacity, access and dimensionality. A substantial amount of data needs to be stored in proper infrastructure and comprehensive analysis which can aid doctors, clinicians, medical experts and families is required. In this study, an investigation of medical data is carried out. We propose an ETL approach to extract features and train machine learning models to predict the post-procedural complications. To derive insights for that, we used well-known clinical dataset named Medical Information Mart for Intensive Care III (MIMIC-III) with two types of data sampling techniques: SMOTE and ADASYN. For both techniques our results showed that Random Forrest outperforms other linear models with an accuracy of greater than 80 percent.**

I. INTRODUCTION

With advancements in digital technologies in medical sciences, different techniques making it possible to explore big data precisely and predict tasks of clinicians, labs and doctors using patient records of diagnoses or procedures. Diagnostic and medical technologies have evolved rapidly and doctors have to take complex decisions. Unfortunately, majority of clinical decisions are not based on evidence. According to 2012 Institute of Medical Committee Report, a small percentage of decision were evidence based. This problem ranges to not have proper clinical guidelines.......

In this paper, we implemented an ETL technique motivated from the different methodologies of ETL techniques [15], [16], which obtain data from original source to perform informative analysis and features extraction to extract features against not so rare diagnoses and procedures with defined ETL process, balancing of our dataset using distributions and sampling techniques and predict 996 (complication or no complication).

The International Classification of Diseases (ICD) [17] is the foundation which identifies and evaluates the statistics of diseases globally. Creates standards for all the diagnoses, diseases which further can be used for research purposes. Under revision of ICD9 codes, the code 996 defines complications particular to certain specified procedures and diagnoses. Most complications are caused due to cardiac, vascular or other used devices and some of them relates to reaction caused due to a procedure performed. In our work, we are focusing on such complications and investigating if those can lead to the mortality of patient. HIPAA (Health Insurance Portability and Accountability Act of 1996) [37] provides privacy and protection of health records for safeguarding and protecting (PHI) medical information. To protect health information MIMIC-III provided anonymized data, still we need to make sure we are following HIPPA compliance rules so that our research does not conflict with any of the standards defined.

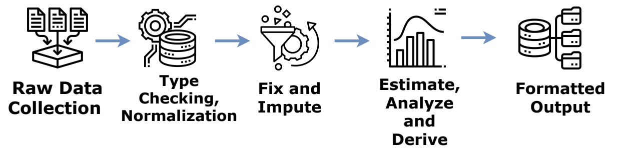

Fig. 1: Learning curve with high loss spikes that excessively perturb a trainable parameter distribution. Losses decrease after loss spikes as parameters are updated back to an intelligent distribution. The learning curve is 2500 iteration boxcar averaged.

A predictor that can evaluate complications using the EHR can help hospital administrators, experts, families and doctors to take decisions that are required for the safety of the patient. For any hospital if the management already knows the precise expected stay of patient they can plan better to use their resources to provide the best possible care. For doctors predictors can evidence, statistics and labels which can be used for taking valuable decisions, for families who will pay for the expenses against the patient can better plan their billing using such predictors.

In our effort, we used Medical Information Mart for Intensive Care MIMIC-III [1]. MIMIC-III is a large, freely-available relational database comprising de-identified [38] health related data associated with over forty thousand patients who stayed in Intensive Care Units at Beth Israel Deaconess Medical Center (Boston, Massachusetts). The data spans June 2001 October2012. The ETL and predicting methods used demographics, data from different hospital systems, lab events, diagnoses, notes and other engineered information regarding each patient.

After the pre-processing step, we used two data sampling techniques: SMOTE and ADASYN and applied Logistic Regression, Random Forrest, Linear SVC and Neural Network to predict the post-procedural complications and accuracy results of all the models were recorded.

The paper is organized as follow: In section II, we explain the methods and frameworks used. In section III, we describe our experimental setup and execution of models. Further, we discussed the significance of results in section IV and concluded the paper in section V.

[1]Jeffrey is a PhD student in Materials and Analytical Sciences, University of Warwick, CV4 7AL Email: j.m.ede@warwick.ac.uk

[2]Richard is a Reader in the Deparment of Physics, University of Warwick, CV4 7AL Email: r.beanland@warwick.ac.uk

II. Algorithm

Adaptive learning rate clipping (ALRC, algorithm 1) is designed to addresses the limitations of gradient clipping. Namely, to be computationally inexpensive, effective for any batch size, robust to hyperparameter choices and to preserve backpropagated gradient distributions. Like gradient clipping, it also has to be applicable to arbitrary loss funtions and neural network architectures.

Algorithm 1 Adaptive learning rate clipping (ALRC) of loss spikes. Sensible parameters are $\beta_1 = \beta_2 = 0.999$, $n = 3$ and $\mu_1^2 < \mu_2$.

```
Initialize running means, $\mu_1$ and $\mu_2$, with decay rates, $\beta_1$ and $\beta_2$.
Choose number, $n$, of standard deviations to clip to.
while Training is not finished do
    Infer forward-propagation loss, $L$.
    $\sigma \leftarrow (\mu_2 - \mu_1^2)^{1/2}$
    $L_\text{max} \leftarrow \mu_1 + n\sigma$
    if $L > L_\text{max}$ then
        $L_\text{dyn} \leftarrow \text{stop\_gradient}(L_\text{max}/L)L$
    else
        $L_\text{dyn} \leftarrow L$
    end if
    Optimize network by back-propagating $L_\text{dyn}$.
    $\mu_1 \leftarrow \beta_1\mu_1 + (1-\beta_1)L$
    $\mu_2 \leftarrow \beta_2\mu_2 + (1-\beta_2)L^2$
end while
```

Rather than allowing loss spikes to destabilize learning, ALRC applies the mapping $\eta L \rightarrow \text{stop\_gradient}(L_\text{max}/L)\eta L$ if $L > L_\text{max}$. The function stop_gradient leaves its operand unchanged in the forward pass and blocks gradients in the backwards pass. ALRC adapts the learning rate to limit the effective loss being backpropagated to L_max. The value of L_max is non-trivial for ALRC to complement existing learning algorithms. In addition to training stability and robustness to hyperparameter choices, L_max needs to adapt to losses and learning rates as they vary.

In our implementation, L_max is a number of standard deviations of the loss above its mean and requires five hyperparameters. There are two decay rates, β_1 and β_2, for exponential moving averages used to estimate the mean and standard deviation of the loss and a number, n, of standard deviations. Similar to batch normalization[1], any decay rate close to 1 is effective e.g. $\beta_1 = \beta_2 = 0.999$. Performance does vary slightly with n; however, we find that any $n \approx 3$ is effective. Initial values for the running means, μ_1 and μ_2, where $\mu_1^2 < \mu_2$ also have to be provided. However, any sensible initial estimates larger than their true values are fine as μ_1 and μ_2 will decay to their correct values.

ALRC can be extended to any loss function or batch size. For batch sizes above 1, we apply ALRC to individual losses, while μ_1 and μ_2 are updated with mean losses. ARLC can also be applied to loss summands; such as per pixel errors between generated and reference images, while μ_1 and μ_2 are updated with the mean errors.

III. Experiments: CIFAR-10 Supersampling

To invistagate the ability of ALRC to stabilize learning and its robustness to hyperperameter choices, we performed a series of toy experiments with networks trained to upsample CIFAR-10[2, 3] images to 32×32×3 after downsampling to 16×16×3.

Data pipeline: In order, images were randomly flipped left or right, had their brightness altered, had their contrast altered, were linearly transformed to have zero mean and unit variance and bilinearly downsampled to 16×16×3.

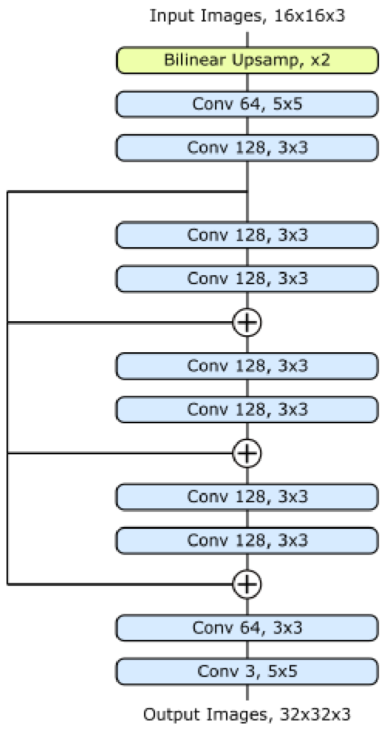

Fig. 2: Convolutional image 2× supersampling network with three skip-2 residual blocks.

Architecture: Images were upsampled and passed through the convolutional network in fig. 2. Each convolutional layer is followed by ReLU[4] activation, except the last.

Initialization: All weights were Xavier[5] initialized. Biases were zero initialized.

Learning policy: ADAM optimization was used with the hyperparameters recommended in [6] and a base learning rate of 1/1280 for 100000 iterations. The learning rate was constant in batch size 1, 4, 16 experiments and decreased to 1/12800 after 54687 iterations in batch size 64 experiments. Networks were trained to minimize mean squared or quartic errors between restored and ground truth images. ALRC was applied to limit the magnitudes of losses to either 2, 3, 4 or ∞ standard deviations above their running means. For batch sizes above 1, ALRC was applied to each loss individually.

Results: Example learning curves for mean squared and quartic error training are shown in fig. 3. Training is more

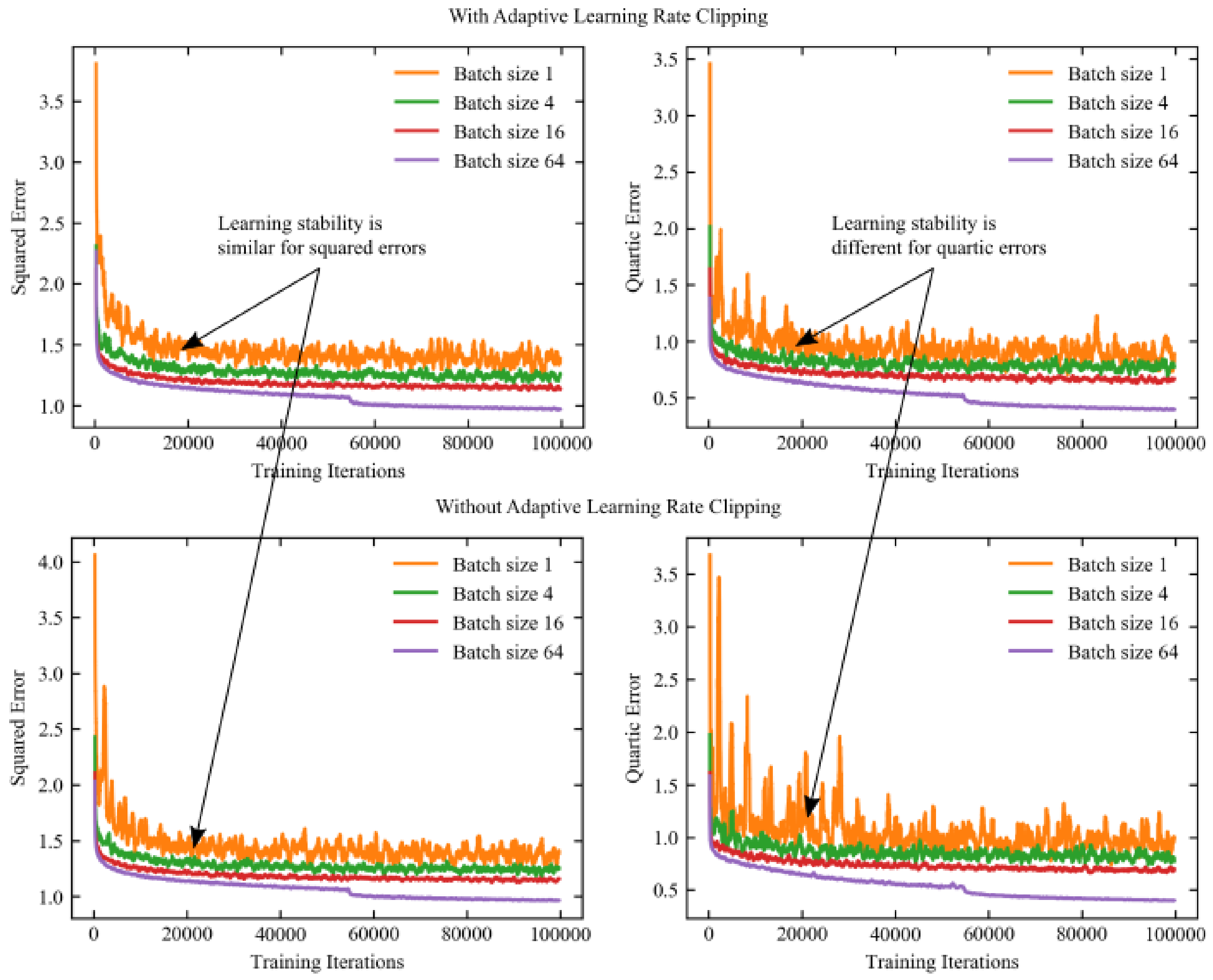

Fig. 3: Unclipped learning curves for 2× CIFAR-10 upsampling with batch sizes 1, 4, 16 and 64 with and without adaptive learning rate clipping of losses to 3 standard deviations above their running means. Training is more stable for squared errors than quartic errors. Learning curves are 500 iteration boxcar averaged.

Squared Errors

	Batch Size 1		Batch Size 4		Batch Size 16		Batch Size 64	
Threshold	Mean	Std Dev	Mean	Std Dev	Mean	Std Dev	Mean	Std Dev
2	5.55	0.048	4.96	0.016	4.58	0.010	-	-
3	5.52	0.054	4.96	0.029	4.58	0.004	3.90	0.013
4	5.56	0.048	4.97	0.017	4.58	0.007	3.89	0.016
∞	5.55	0.041	4.98	0.017	4.59	0.006	3.89	0.014

Quartic Errors

	Batch Size 1		Batch Size 4		Batch Size 16		Batch Size 64	
Threshold	Mean	Std Dev	Mean	Std Dev	Mean	Std Dev	Mean	Std Dev
2	3.54	0.084	3.02	0.023	2.60	0.012	1.65	0.011
3	3.59	0.055	3.08	0.024	2.61	0.014	1.58	0.016
4	3.61	0.054	3.13	0.023	2.64	0.016	1.57	0.016
∞	3.88	0.108	3.32	0.037	2.74	0.020	1.61	0.008

TABLE I: Adaptive learning rate clipping (ALRC) for losses 2, 3, 4 and ∞ running standard deviations above their running means for batch sizes 1, 4, 16 and 64. ARLC was not applied for clipping at ∞. Each squared and quartic error mean and standard deviation is for the means of the final 5000 training errors of 10 experiments. ALRC lowers errors for unstable quartic error training at low batch sizes and otherwise has little effect. Means and standard deviations are multiplied by 100.

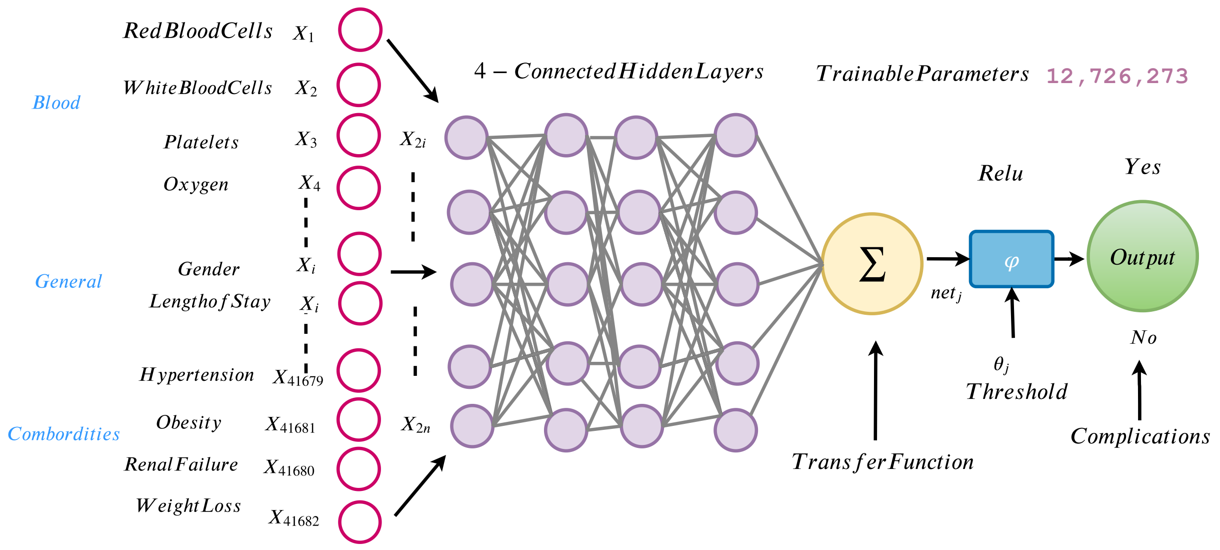

Fig. 4: Neural network completions of 512×512 scanning transmission electron microscopy images from 1/20 coverage blurred spiral scans.

IV. Experiments: Partial-STEM

To test ALRC in practice, we applied our algorithm to neural networks learning to complete 512×512 scanning transmission electron microscopy (STEM) images from partial scans with 1/20 coverage. Example completions are shown in fig. 4.

Data pipeline: In order, each image was subject to a random combination of flips and 90° rotations to augment the dataset by a factor of 8. Next, each STEM images was blurred and a path described by a 1/20 coverage spiral was selected. Finally, artificial noise was added to scans to make them more difficult to complete.

Architecture: Our network can be divided into the three subnetworks shown in fig. 5: an inner generator, outer generator and an auxiliary inner generator trainer. The auxiliary trainer[7, 8] is introduced to provide a more direct path for gradients to backpropagate to the inner generator. Each convolutional layer is followed by ReLU activation, except the last.

Initialization: Weights were initialized from a normal distribution with mean 0.00 and standard deviation 0.05. There are no biases.

Weight normalization: All generator weights are weight normalized[9] and a weight normalization initialization pass was performed after weight initialization. Following [9, 10], running mean-only batch normalization was applied to the output channels of every convolutional layer except the last. Channel means were tracked by exponential moving averages with decay rates of 0.99. Similar to [11], running mean-only batch normalization was frozen in the second half of training to improve stability.

Loss functions: The auxiliary inner generator trainer learns to generate half-size completions that minimize MSEs from half-size blurred ground truth STEM images. Meanwhile, the outer generator learns to produce full-size completions that minimize MSEs from blurred STEM images. All MSEs were multipled by 200. The inner generator cooperates with the auxiliary inner generator trainer and outer generator.

To benchmark ALRC, we investigated training with MSEs, Huberized ($h = 1$) MSEs, MSEs with ALRC and Huberized ($h = 1$) MSEs with ALRC before Huberization. Training with both ALRC and Hubarization showcases the ability of ALRC to complement another loss function modification.

Learning policy: ADAM optimization[6] was used with a constant generator learning rate of 0.0003 and a first moment of the momentum decay rate, $\beta_1 = 0.9$, for 250000 iterations. In the next 250000 iterations, the learning rate and β_1 were linearly decayed in eight steps to zero and 0.5, respectively. The learning rate for the auxiliary inner generator trainer was two times the generator learning rate; β_1 were the same. All training was performed with batch size 1 due to the large model size needed to complete 512×512 scans.

Results: Outer generator losses in fig. 6 show that ALRC and Huberization stabilize learning. Further, ALRC accelerates MSE and Huberized MSE convergence to lower losses. To be clear, learning policy was optimized for MSE training so direct loss comparison is uncharitable to ALRC.

V. Discussion

Taken together, our CIFAR-10 supersampling results show that ALRC improves stability and lowers losses for learning that would be destabilized by loss spikes and otherwise has little effect. Loss spikes are often encountered when training with high learning rates, high order loss functions or small batch sizes. However, a moderate learning rate was used in MSE experiments so losses did not spike enough to destabilize learning. In contrast, mean quartic error training is unstable so ALRC stabilizes training and lowers losses.

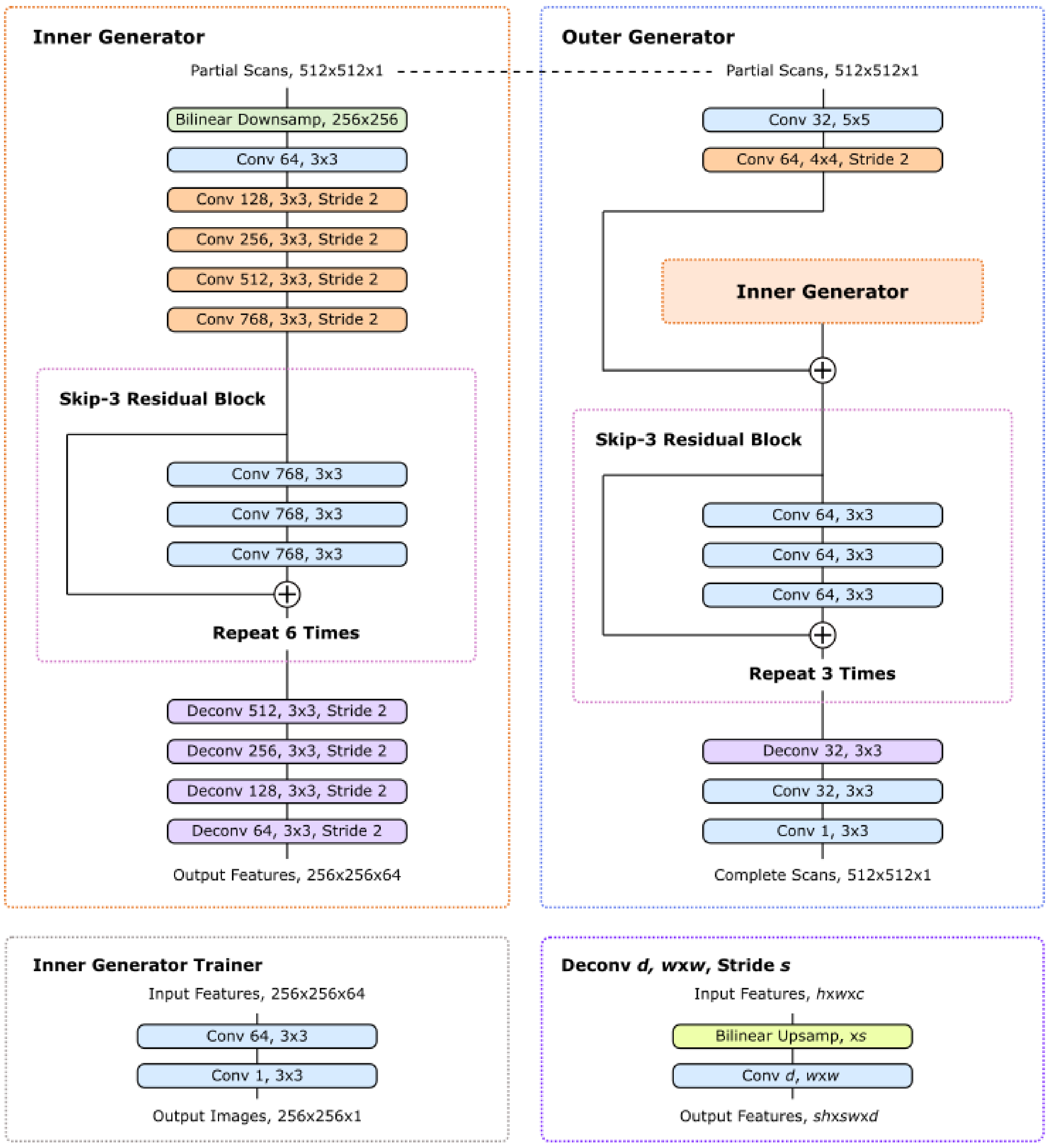

Fig. 5: Two-stage generator that completes 512×512 micrographs from partial scans. A dashed line indicates that the same image is input to the inner and outer generator. Large scale features developed by the inner generator are locally enhanced by the outer generator and turned into images. An auxiliary inner generator trainer restores images from inner generator features to provide direct feedback.

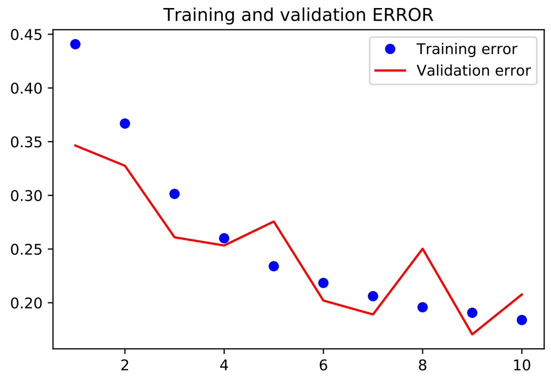

Fig. 6: Outer generator losses show that ALRC and Huberization stabilize learning. ALRC lowers final mean squared error (MSE) and Huberized MSE losses and accelerates convergence. Learning curves are 2500 iteration boxcar averaged.

Similar results are confirmed for partial-STEM where ALRC stabilizes learning and lowers losses.

ALRC is designed to complement existing learning algorithms with new functionality. It is effective for any loss function or batch size and can be applied to any neural network trained with a variant of stochastic gradient descent. Our algorithm is also computationally inexpensive, requiring orders of magnitude fewer operations than other layers typically used in neural networks. As ALRC either stabilizes learning or has little effect, this means that it is suitable for routine application to arbitrary neural network training with SGD. In addition, we note that ALRC is a simple algorithm that has a clear effect on learning.

Nevertheless, ALRC can replace other learning algorithms in some situations. For instance, ALRC is a computationally inexpensive alternative to gradient clipping in high batch size training where gradient clipping is being used to limit perturbations by loss spikes. However, it is not a direct replacement as ALRC preserves the distribution of backpropagated gradients whereas gradient clipping reduces large gradients. Instead, ALRC is designed to complement gradient clipping by limiting perturbations by large losses while gradient clipping modifies gradient distributions.

The implementation of ALRC in algorithm 1 is for positive losses. This avoids the need to introduce small constants to prevent divide-by-zero errors. Nevertheless, ALRC can support negative losses by using standard methods to prevent divide by zero errors. Alternatively, a constant can be added to losses to make them positive without affecting learning.

ALRC can also be extended to limit losses more than a number of standard deviations below their mean. This had no effect in our experiments. However, preemptively reducing loss spikes by clipping rewards between user-provided upper and lower bounds can improve reinforcement learning[12]. Subsequently, we suggest that clipping losses below their means did not improve learning because losses mainly spiked above their means; not below. Some partial-STEM losses did spike below; however, they were mainly for blank or otherwise trivial completions.

VI. Conclusions

We have developed ALRC to stabilize the training of artificial neural networks by limiting backpropagated losses. Our experiments show that ALRC accelerates convergence and lowers losses for learning that would be destabilized by loss spikes and otherwise has little effect. Further, ALRC is computationally inexpensive, can be applied to any loss function or batch size, does not affect the distribution of backpropagated gradients and has a clear effect on learning. Overall, ALRC complements existing learning algorithms and can be routinely applied to arbitrary neural network training with SGD.

VII. Source Code

Source code for CIFAR-10 supersampling experiments and a TensorFlow[13] implementation of ALRC is available at https://github.com/faisalmaqbool94/Predicting-Post-Procedural-Complications-Using-MIM

References

[1] S. Ioffe and C. Szegedy, "Batch normalization: Accelerating deep network training by reducing internal covariate shift," *arXiv preprint arXiv:1502.03167*, 2015.
[2] A. Krizhevsky, V. Nair, and G. Hinton, "The cifar-10 dataset," *online: http://www.cs.toronto.edu/~kriz/cifar.html*, vol. 55, 2014.
[3] A. Krizhevsky and G. Hinton, "Learning multiple layers of features from tiny images," tech. rep., Citeseer, 2009.
[4] V. Nair and G. E. Hinton, "Rectified linear units improve restricted boltzmann machines," in *Proceedings of the 27th international conference on machine learning (ICML-10)*, pp. 807–814, 2010.
[5] X. Glorot and Y. Bengio, "Understanding the difficulty of training deep feedforward neural networks," in *Proceedings of the thirteenth international conference on artificial intelligence and statistics*, pp. 249–256, 2010.
[6] D. P. Kingma and J. Ba, "Adam: A method for stochastic optimization," *arXiv preprint arXiv:1412.6980*, 2014.
[7] C. Szegedy, W. Liu, Y. Jia, P. Sermanet, S. Reed, D. Anguelov, D. Erhan, V. Vanhoucke, and A. Rabinovich, "Going deeper with convolutions, corr abs/1409.4842," *URL http://arxiv.org/abs/1409.4842*, 2014.
[8] C. Szegedy, V. Vanhoucke, S. Ioffe, J. Shlens, and Z. Wojna, "Rethinking the inception architecture for computer vision. arxiv 2015," *arXiv preprint arXiv:1512.00567*, vol. 1512, 2015.
[9] T. Salimans and D. P. Kingma, "Weight normalization: A simple reparameterization to accelerate training of deep neural networks," in *Advances in Neural Information Processing Systems*, pp. 901–909, 2016.
[10] E. Hoffer, R. Banner, I. Golan, and D. Soudry, "Norm matters: efficient and accurate normalization schemes in deep networks," in *Advances in Neural Information Processing Systems*, pp. 2160–2170, 2018.
[11] L.-C. Chen, G. Papandreou, F. Schroff, and H. Adam, "Rethinking atrous convolution for semantic image segmentation," *arXiv preprint arXiv:1706.05587*, 2017.
[12] V. Mnih, K. Kavukcuoglu, D. Silver, A. A. Rusu, J. Veness, M. G. Bellemare, A. Graves, M. Riedmiller, A. K. Fidjeland, G. Ostrovski, *et al.*, "Human-level control through deep reinforcement learning," *Nature*, vol. 518, no. 7540, p. 529, 2015.
[13] M. Abadi, P. Barham, J. Chen, Z. Chen, A. Davis, J. Dean, M. Devin, S. Ghemawat, G. Irving, M. Isard, *et al.*, "Tensorflow: A system for large-scale machine learning.," in *OSDI*, vol. 16, pp. 265–283, 2016.

VIII. Acknowledgements

This research was funded by EPSRC grant EP/N035437/1.